Supporting Information

LiFSA-KFSA Binary Molten Salt Enables Durable Lithium-antimony Batteries at 80-100 °C

Jinling Zhong[a,b], Shixin He[a,b], Yucheng Zhang[a,b], Wenjian Wang[a], Yuxuan Zhang[a], Wen Wen[c], Linjuan Zhang[a], Yao Liu[a,*], Yonggang Wang[d,*] and Jian-Qiang Wang[a,*]

[a]State Key Laboratory of Thorium Energy, Shanghai Institute of Applied Physics, Chinese Academy of Sciences, No. 2019 Jialuo Road, Jiading District, Shanghai 201800, P. R. China

[b]University of Chinese Academy of Sciences, Yuquanlu Campus, No.19A Yuquan Road, Shijingshan District, Beijing 100049, P. R. China

[c]Shanghai Synchrotron Radiation Facility, Shanghai Advanced Research Institute, Chinese Academy of Sciences, No. 99 Haike Road, Zhangjiang Hi-tech Park, Pudong, Shanghai 201204, P. R. China

[d]Department of Chemistry, Fudan University, 2005 Songhu Road, Yangpu District, Shanghai 201204, P. R. China

*e-mail: liuyao@sinap.ac.cn; ygwang@fudan.edu.cn; wangjianqiang@sinap.ac.cn

Experiments

Materials

Antimony (Sb, ≥99.5%), lithium bis(fluorosulfonyl)imide (LiFSA, 99%), and bis(fluorosulfonyl)imide potassium salt (KFSA, ≥95%) were supplied by Shanghai Aladdin Biochemical Technology Co., Ltd. TUBALL™ BATT dispersion (containing 99.0 wt.% H_2O, 0.6 wt.% sodium carboxymethyl cellulose, and 0.4 wt.% single-walled carbon nanotubes) was obtained from OCSiAl (Shenzhen) Co., Ltd. A glass fiber separator (GF-A, Whatman) was purchased from Dongguan Canrd New Energy Technology Co., Ltd. To prepare a mixed salt with a molar ratio of 45 : 55 ($Li_{0.45}K_{0.55}FSA$, denoted as LiKFSA), LiFSA and KFSA were manually ground in an agate mortar for 30 minutes at a molar ratio of 45 : 55 until a homogeneous powder was obtained. 1.0 M lithium hexafluorophosphate ($LiPF_6$) in ethylene carbonate (EC) : dimethyl carbonate (DMC) = 1 : 1 wt. % supplied from Suzhou DuoDuo Chemical Technology Co., Ltd.

Physical Characterizations

The surface and cross-sectional morphologies of the electrodes were examined using a Zeiss Crossbeam 540 (Germany) scanning electron microscope (SEM) equipped with energy-dispersive X-ray spectroscopy (EDS). X-ray diffraction (XRD) patterns were collected on a Bruker D8 Advance diffractometer (Germany) with Cu $K\alpha$ radiation (λ = 1.5406 Å) over a 2θ range of 20-90°. Surface elemental composition and chemical states were analyzed by X-ray photoelectron spectroscopy (XPS, Thermo Fisher Scientific, Czech Republic). All binding energies were calibrated against the adventitious carbon C 1s peak at 284.8 eV, and data were processed using the Avantage software. Time-of-flight secondary ion mass spectrometry (TOF-SIMS) depth profiling was performed on a PHI nanoTOF III instrument (Physical Electronics, USA). A pulsed 30 kV Bi_3++ primary ion beam was used for analysis over a 50 × 50 μm^2 area. For depth profiling, a 2 kV Cs sputter gun rastered over

400 × 400 μm^2 to maintain a flat crater bottom, with a sputtering rate calibrated at 0.18 nm s^{-1} relative to SiO_2. All spectra were acquired in negative polarity mode across a mass range of 0-1850 amu.

To mitigate the air exposure of Sb electrode, all post-cycling cells were disassembled in an argon-filled glovebox. The harvested electrodes were subsequently transferred to the analysis chambers using an airtight vessel for subsequent TOF-SIMS and XPS characterization.

In-situ X-ray absorption near-edge spectroscopy (XANES) measurements were conducted in transmission mode at the BL13SSW beamline of the Shanghai Synchrotron Radiation Facility (SSRF). Data were processed using the Athena software for background subtraction and normalization. *In-situ* synchrotron XRD (SXRD) experiments were performed at the BL03HB beamline of the SSRF with a monochromatic incident X-ray energy of 18.0 keV (λ = 0.6888 Å). Diffraction patterns were recorded in transmission geometry using a large-area 2D detector placed 450 mm from the sample. The detector distance and wavelength were calibrated with a LaB_6 standard. During electrochemical cycling, SXRD frames were collected continuously at a time resolution of 1 minute per frame. The resulting 2D diffraction rings were integrated into 1D intensity-2θ profiles using Fit2D software. A modified 2032-coin cell with a 5 mm aperture was employed. A polyimide (PI) film served as both a seal for the cell and a window for the synchrotron light source. The cell was integrated with an electrochemical workstation and a temperature-controlled heating device. During the testing process, the temperature was ramped up to 90 °C at a heating rate of 10 °C min^{-1}, followed by a 30 min rest period. Subsequently, the cell underwent galvanostatic charge-discharge testing at a C/2 rate while simultaneously conducting XANES and SXRD measurements. In addition, we verified that the perforated coin cell and the standard coin cell exhibited the same electrochemical performance to ensure reliable operando measurements.

Electrochemical Measurements

Sb powder was mixed with TUBALL™ BATT dispersion in a weight ratio of 9 : 1 via ball milling for 25 minutes to form a homogeneous slurry. The slurry was coated onto copper foil and dried under vacuum at 60 °C for 10 h. The resulting electrodes were punched into 12 mm discs with an active material loading of approximately 0.5 mg cm^{-2}. Coin cells (2032-type) were assembled in an argon-filled glove box (H_2O < 0.01 ppm, O_2 < 0.01 ppm) using the prepared electrode as the cathode, lithium metal as the anode, and a glass-fiber separator. Prior to assembly, the LiKFSA electrolyte was heated to 80 °C to ensure complete melting and homogeneity. Each cell was filled with 100 mg of the molten salt. The sealed cells were then stored at the designated test temperatures of 80 °C, 90 °C, or 100 °C. Galvanostatic charge-discharge tests were conducted on a Land CT3004A battery test system within a voltage window of 0.6-1.8 V. All cells were initially activated for three cycles at C/10 between 0.01 and 2 V.

In-situ electrochemical impedance spectroscopy (EIS) was performed using a Biologic SP-300 electrochemical workstation over a frequency range of 1 MHz to 0.1 Hz with an AC amplitude of 5.0 mV.

The energy density and power density were calculated based on the following equations:

$$Energy\ density\ (Wh\ kg^{-1}) = \frac{Discharge\ capacity\ (mAh) \times Average\ discharge\ voltage\ (V)}{Mass\ of\ active\ materials}$$

$$Power\ density\ (W\ kg^{-1}) = \frac{Dicharge\ current\ (mA) \times Average\ discharge\ voltage\ (V)}{Mass\ of\ active\ materials}$$

The mass of active materials refers to the total mass of the cathode and anode. The calculated value was then multiplied by 70% (assuming inactive materials account for 30% of the total mass).

The Li^+ transference number (t_{Li^+}) was evaluated using a symmetric Li||Li cell via a combination of EIS and chronoamperometry. A constant polarization voltage (ΔV) of 10 mV was applied, and the initial (I_0) and steady-state (I_s) currents were recorded. The corresponding interfacial resistances

before (R_0) and after (R_s) polarization were obtained from EIS. The transference number was calculated using equation (1):

$$t_{Li^+} = \frac{I_s(\Delta V - I_0 R_0)}{I_0(\Delta V - I_s R_s)} \qquad (1)$$

Ionic conductivity (σ) of the separator was determined using symmetric stainless-steel (SS||SS) cells, wherein the GF-A separator was impregnated with 100 mg of molten salt. The conductivity was calculated according to equation (1):

$$\sigma = \frac{L}{S \times R} \qquad (2)$$

where R is the bulk resistance derived from the EIS spectrum, S is the electrode area, and L is the thickness of the separator.

Galvanostatic intermittent titration technique (GITT) measurements were conducted on the Land CT3004A system at 80, 90, and 100 °C. Each cell was pulsed at C/10 for 10 minutes, followed by a 30 minutes relaxation period to allow voltage equilibration. This sequence was repeated across the voltage range of 0.6-1.8 V during both charge and discharge. The lithium diffusion coefficient of the active material can be calculated by the following equation (3):

$$D^{GITT} = \frac{4}{\pi\tau}\left(\frac{m_B V_M}{M_B S}\right)^2 \left(\frac{\Delta E_s}{\Delta E_t}\right)^2 \qquad (3)$$

Here, τ represents the pulse duration; Sdenotes the active surface area of the electrode; and m_B, M_B, and V_M correspond to the mass, molar mass, and molar volume of the active material, respectively (note that the term $m_B V_M / M_B$ yields the volume of the electrode). Furthermore, ΔE_s is the change in steady-state voltage for a single step, while ΔE_t refers to the total voltage change during the pulse.

Cyclic voltammetry (CV) was carried out on a Biologic SP-300 workstation. For the initial cycle, scans were recorded between 0.01 and 2 V vs. Li/Li+ at a rate of 0.1 mV s−1. To distinguish capacitive from diffusion-controlled contributions, additional CV profiles were collected at various scan rates (0.1, 0.3, 0.5, 0.7, 0.9, 1.5, 3, 6, and 10 mV s−1). The current-scan rate relationship follows the power-law expression (4):

$$i = av^b \qquad (4)$$

where $b = 1$ indicates a capacitive-dominated process and $b = 0.5$ suggests a diffusion-controlled process. When both mechanisms coexist, the current can be deconvoluted using:

$$i = k_1 v + k_2 v^{1/2} \qquad (5)$$

where k_1 and k_2 are voltage dependent fitting parameters. All CV tests were performed at 80, 90, and 100 °C, respectively.

Supplementary Figures

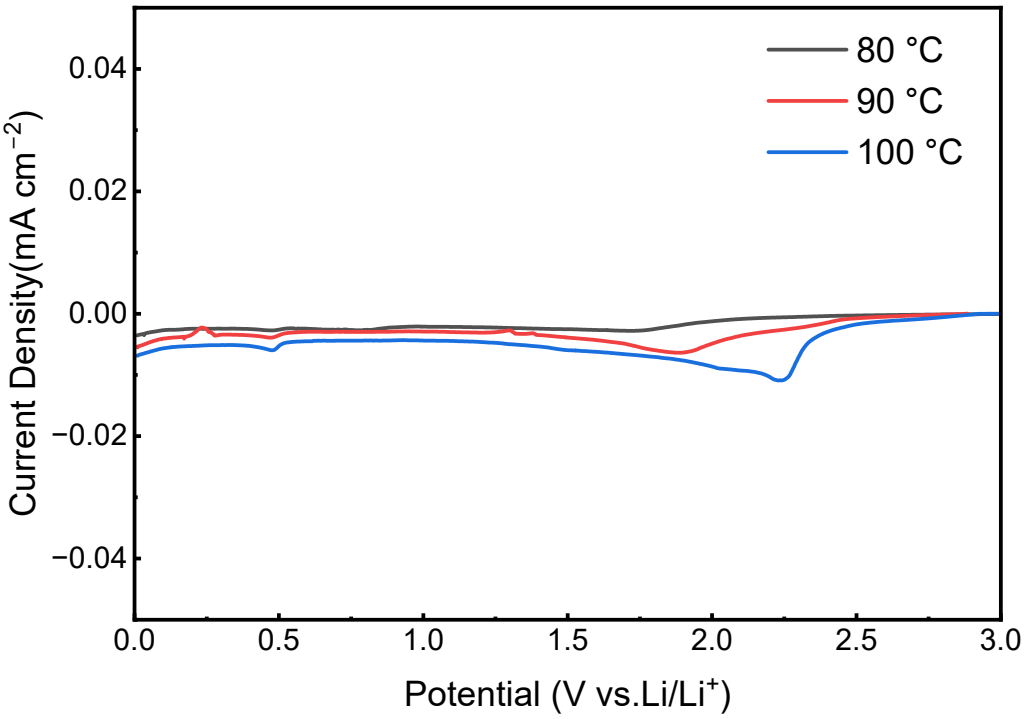

Figure S1. Linear sweep voltammetry (LSV) was performed at 0.1 mV s^{-1} on Li||SS coin cells containing a molten salt electrolyte at 80, 90, and 100 °C.

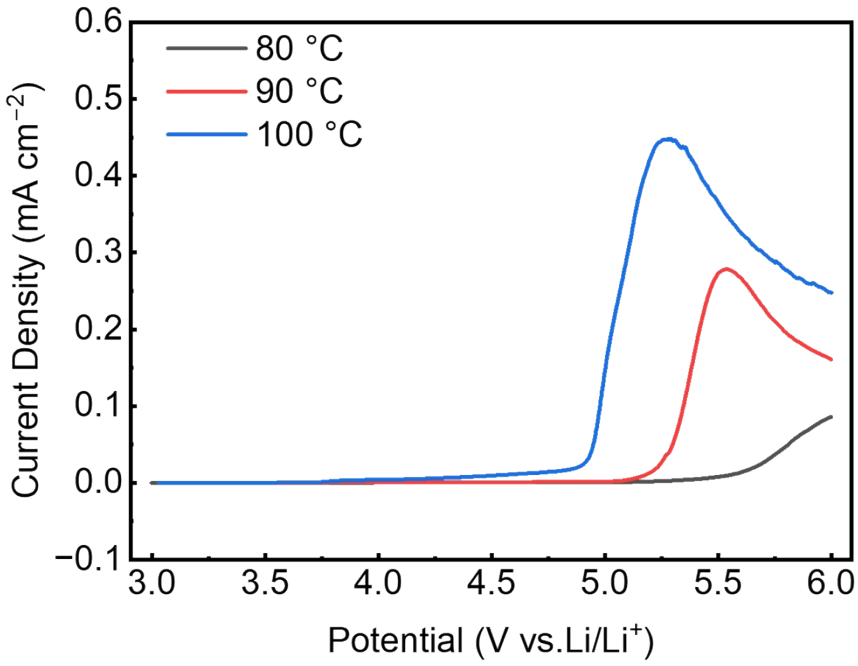

Figure S2. Linear sweep voltammetry (LSV) was performed at 0.1 mV s^{-1} on Li||SS coin cells containing a molten salt electrolyte at 80, 90, and 100 °C.

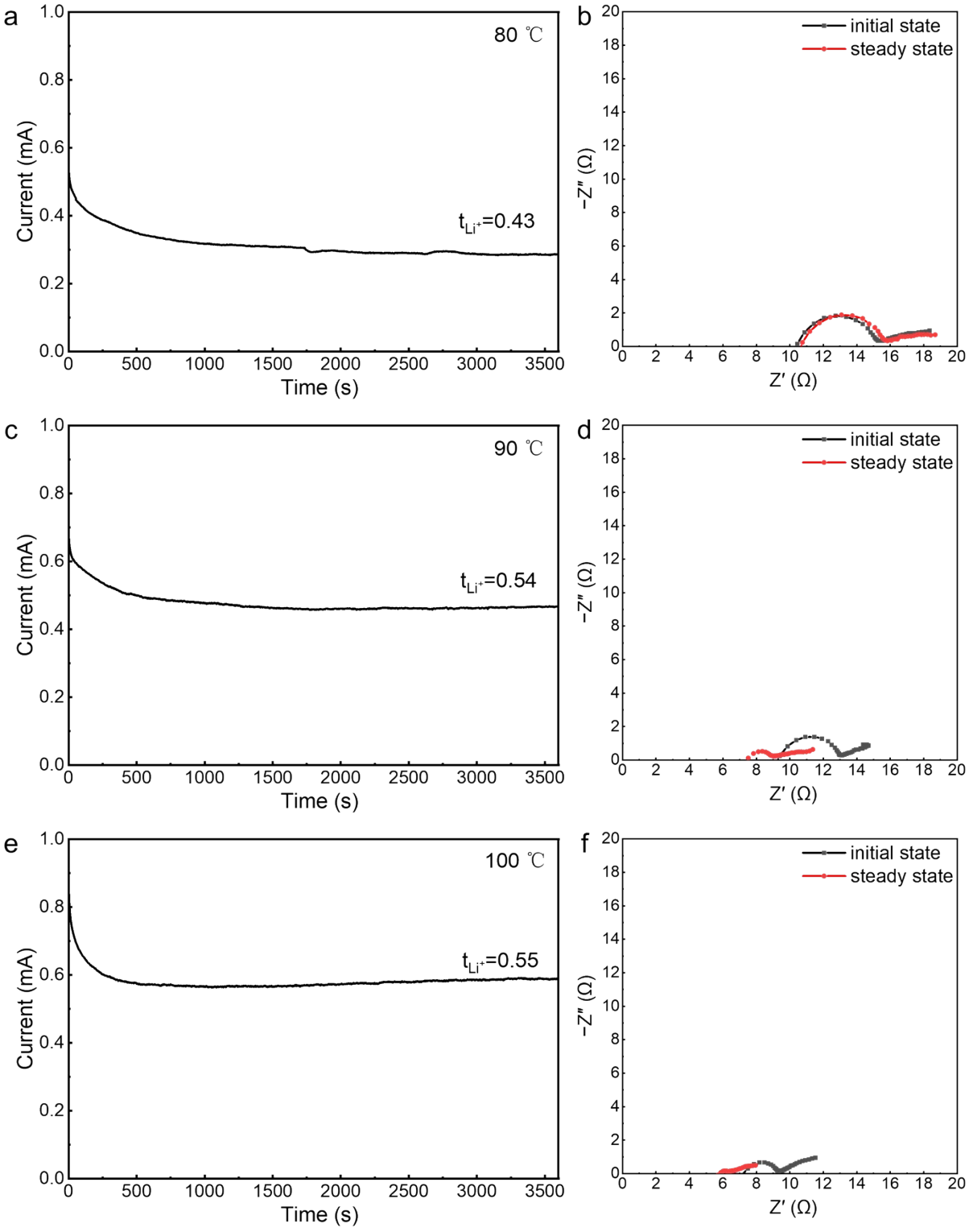

Figure S3. (a-f) Electrochemical testing (Li^+ transference number), Li||Li symmetrical cell at 80, 90, and 100 °C. The potentiostatic polarization method/constant current electrolytic analysis.

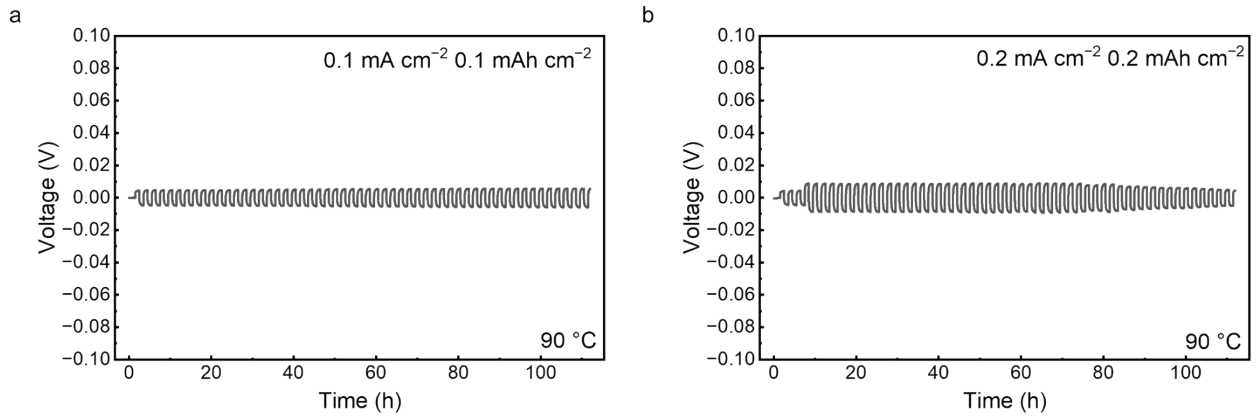

Figure S4. Cycling performance of Li||Li symmetric cells at 90 °C. a) 0.1 mA cm^{-2}, 0.1 mAh cm^{-2}; b) 0.2 mA cm^{-2}, 0.2 mAh cm^{-2}.

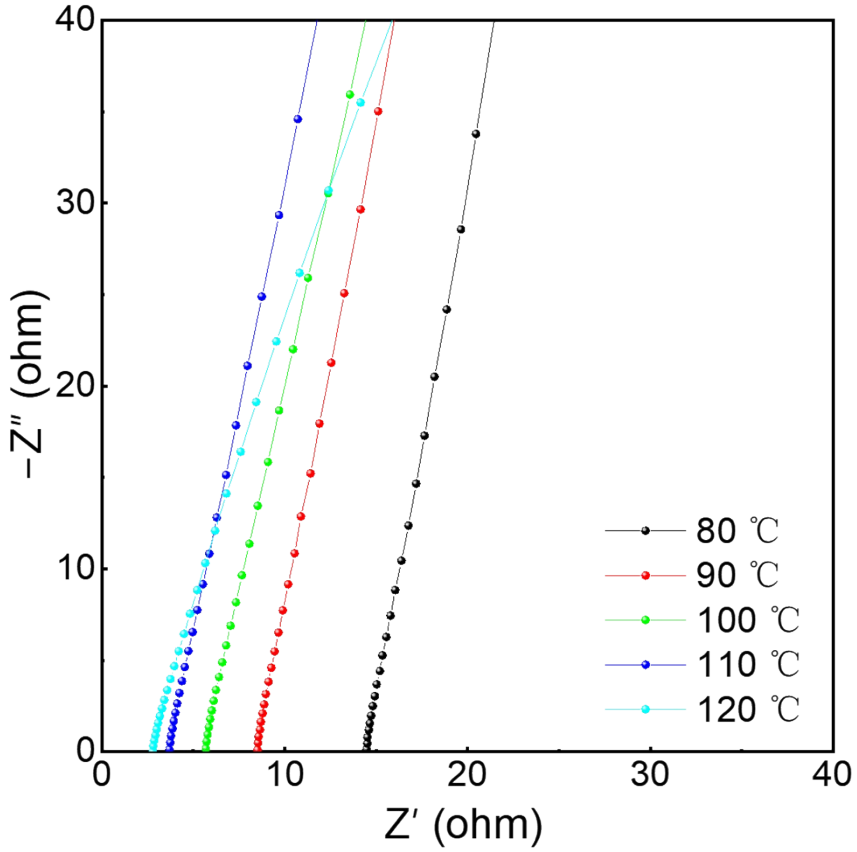

Figure S5. EIS Nyquist plots of SS||SS symmetrical cell in LiKFSA molten salt electrolyte at 80, 90, 100, 110, and 120 °C. Electrochemical Impedance Spectroscopy (0.1-10^6 Hz, 5 mV).

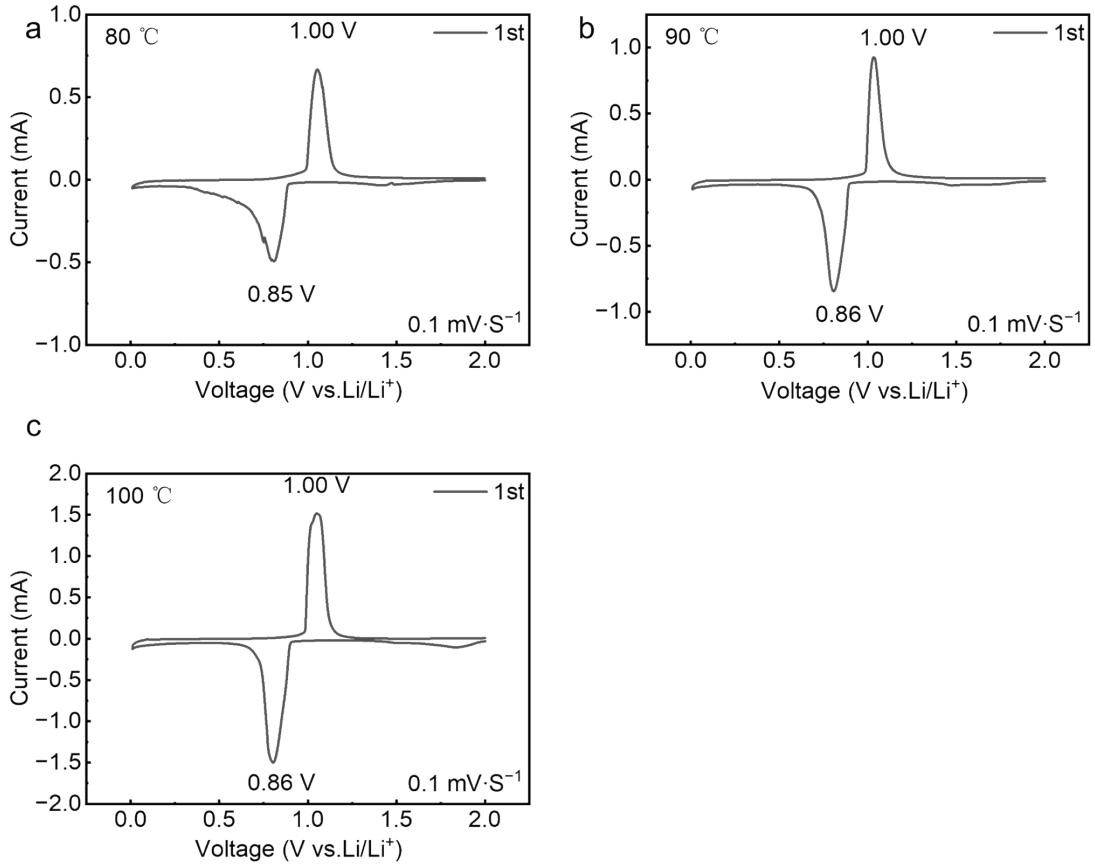

Figure S6. (a-c) CV curves. Li||Sb LiKFSA molten salt batteries for initial cycles at 80, 90, and 100 °C under a scanning rate of 0.1 mV s^{-1} in the voltage window of 0.01 to 2.0 V.

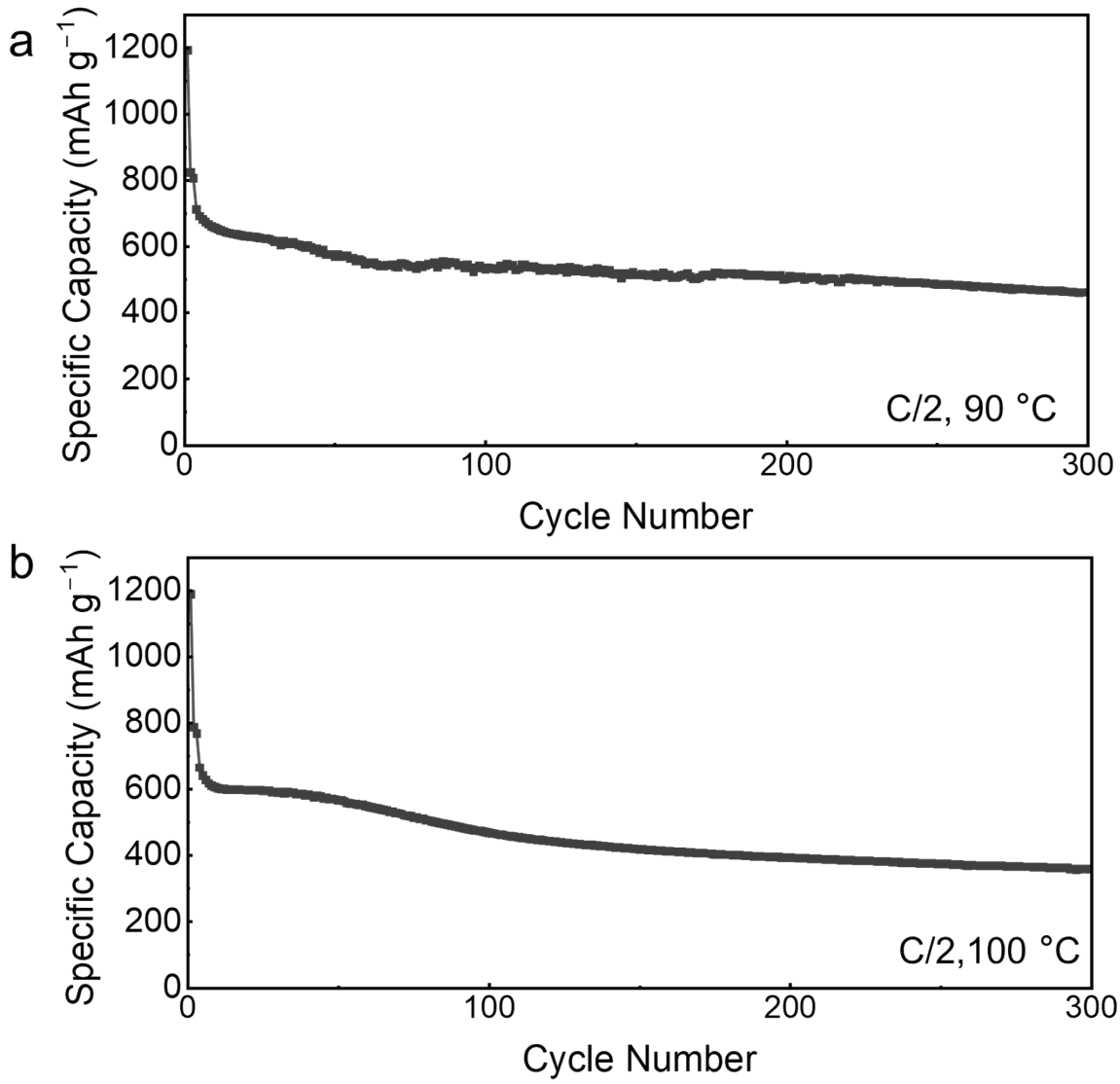

Figure S7. (a, b) Specific Capacity vs. Cycle Number at C/2 at 90 °C and 100 °C of Li||Sb molten salt batteries.

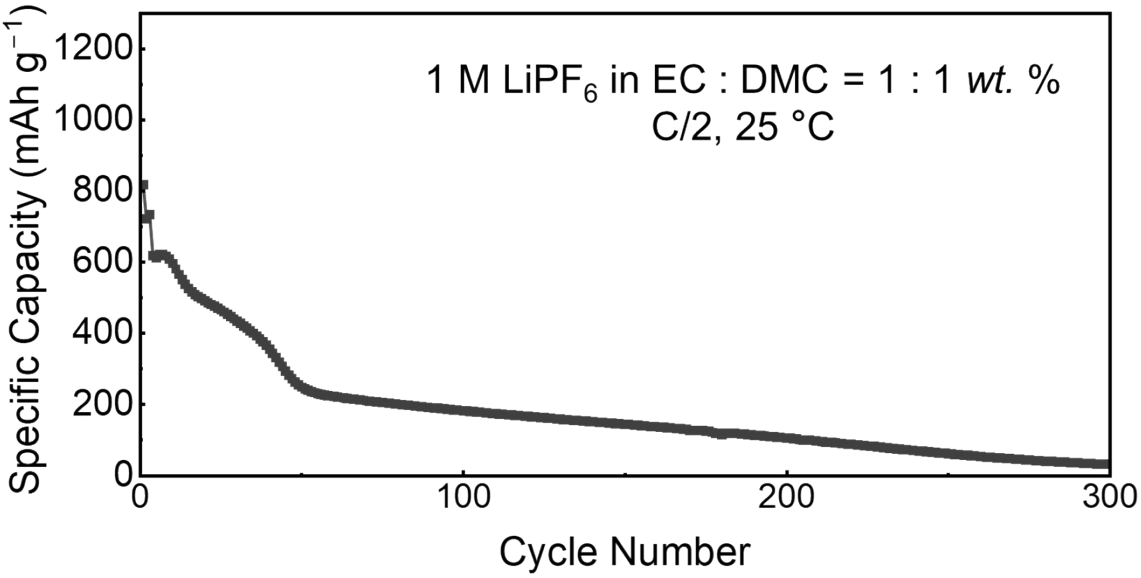

Figure S8. Specific Capacity vs. Cycle Number at C/2 at 25 °C in conventional organic liquid electrolyte (1 M $LiPF_6$ in EC : DMC = 1: 1 wt. %) of Li||Sb batteries.

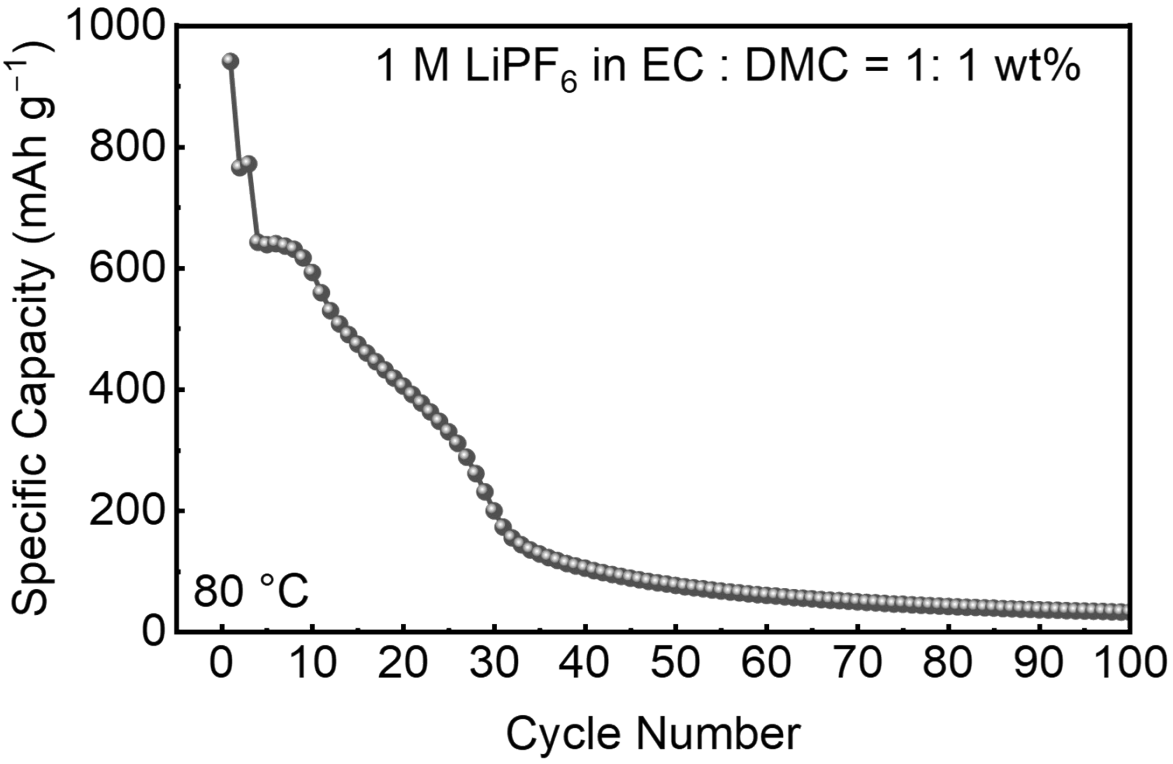

Figure S9. Specific Capacity vs. Cycle Number at 5 C at 80 °C in conventional organic liquid electrolyte (1 M $LiPF_6$ in EC : DMC = 1: 1 wt. %) of Li||Sb batteries.

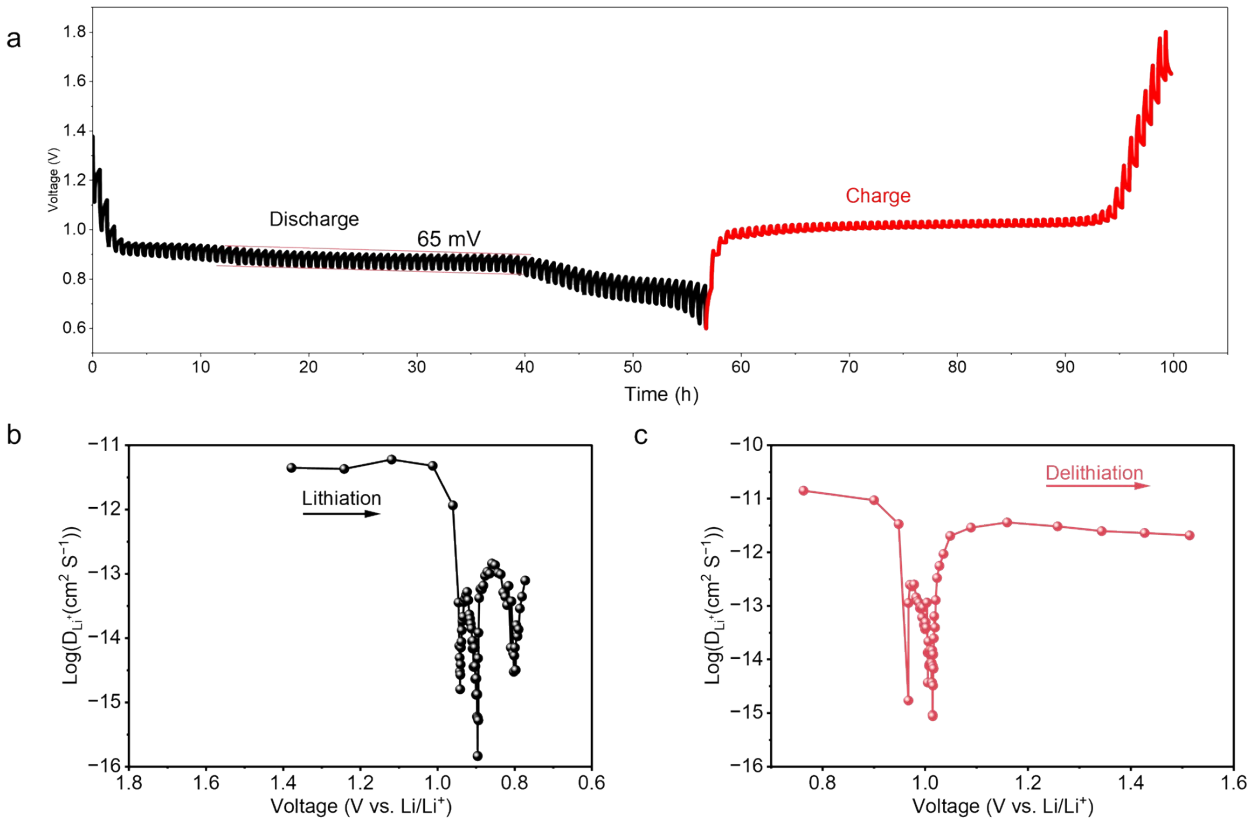

Figure S10. (a) kinetics of electrochemical reaction using GITT, at 80 °C. The GITT was tested under a current rate of C/10 within 0.6 V-1.8 V using a current pulse of 10 minutes, followed by a relaxation time of 30 minutes. **(b, c)** The cucullated lithium-ion diffusion during the lithiation and delithiation process.

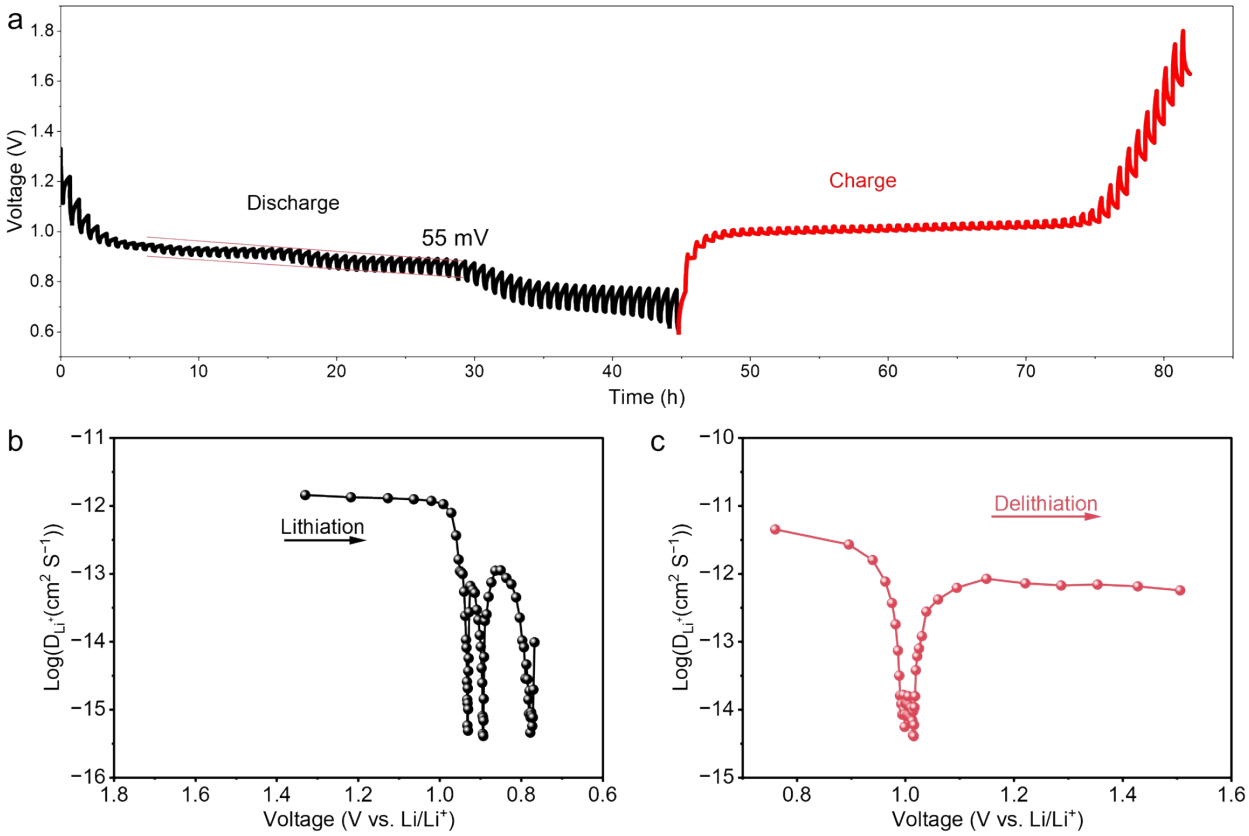

Figure S11. (a) kinetics of electrochemical reaction using GITT, at 90 °C. The GITT was tested under a current rate of C/10 within 0.6 V-1.8 V using a current pulse of 10 minutes, followed by a relaxation time of 30 minutes. **(b, c)** The cucullated lithium-ion diffusion during the lithiation and delithiation process.

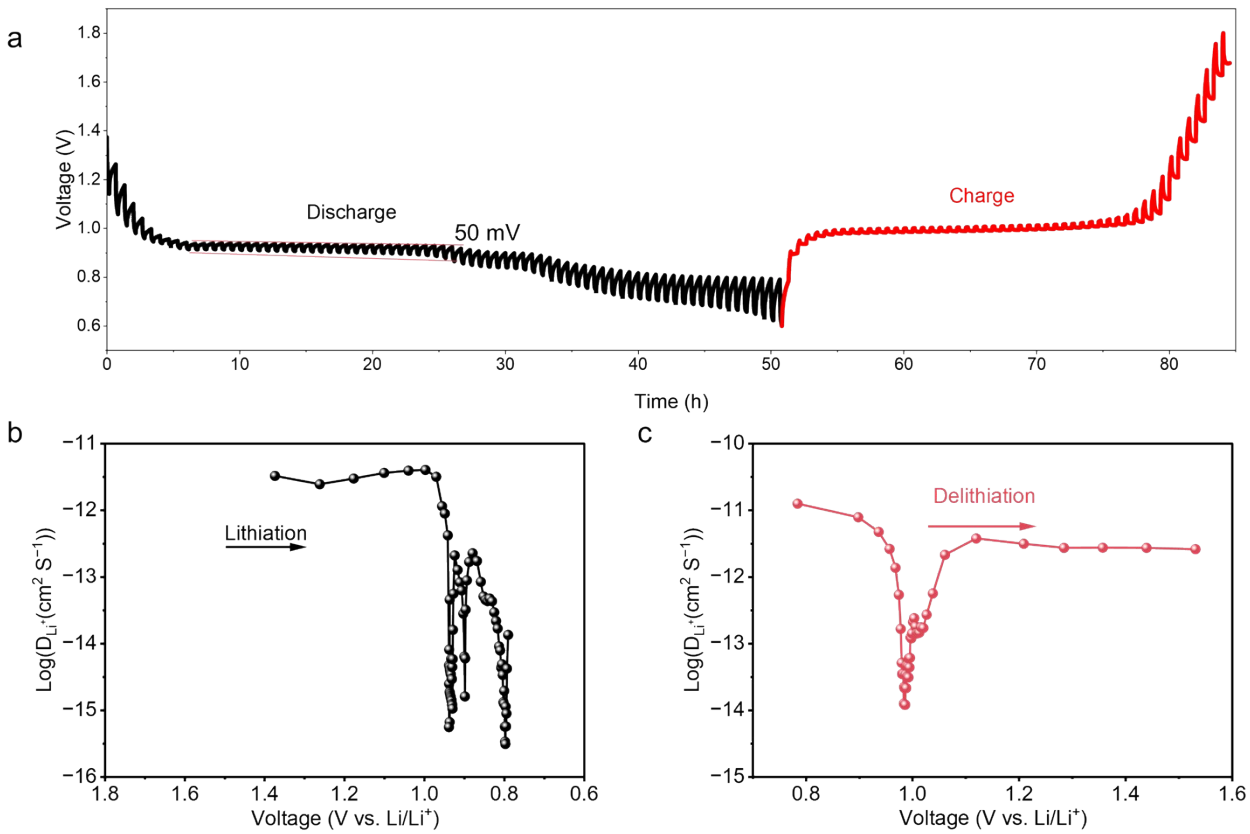

Figure S12. (a) kinetics of electrochemical reaction using GITT, at 100 °C. The GITT was tested under a current rate of C/10 within 0.6 V-1.8 V using a current pulse of 10 minutes, followed by a relaxation time of 30 minutes. **(b, c)** The cucullated lithium-ion diffusion during the lithiation and delithiation process.

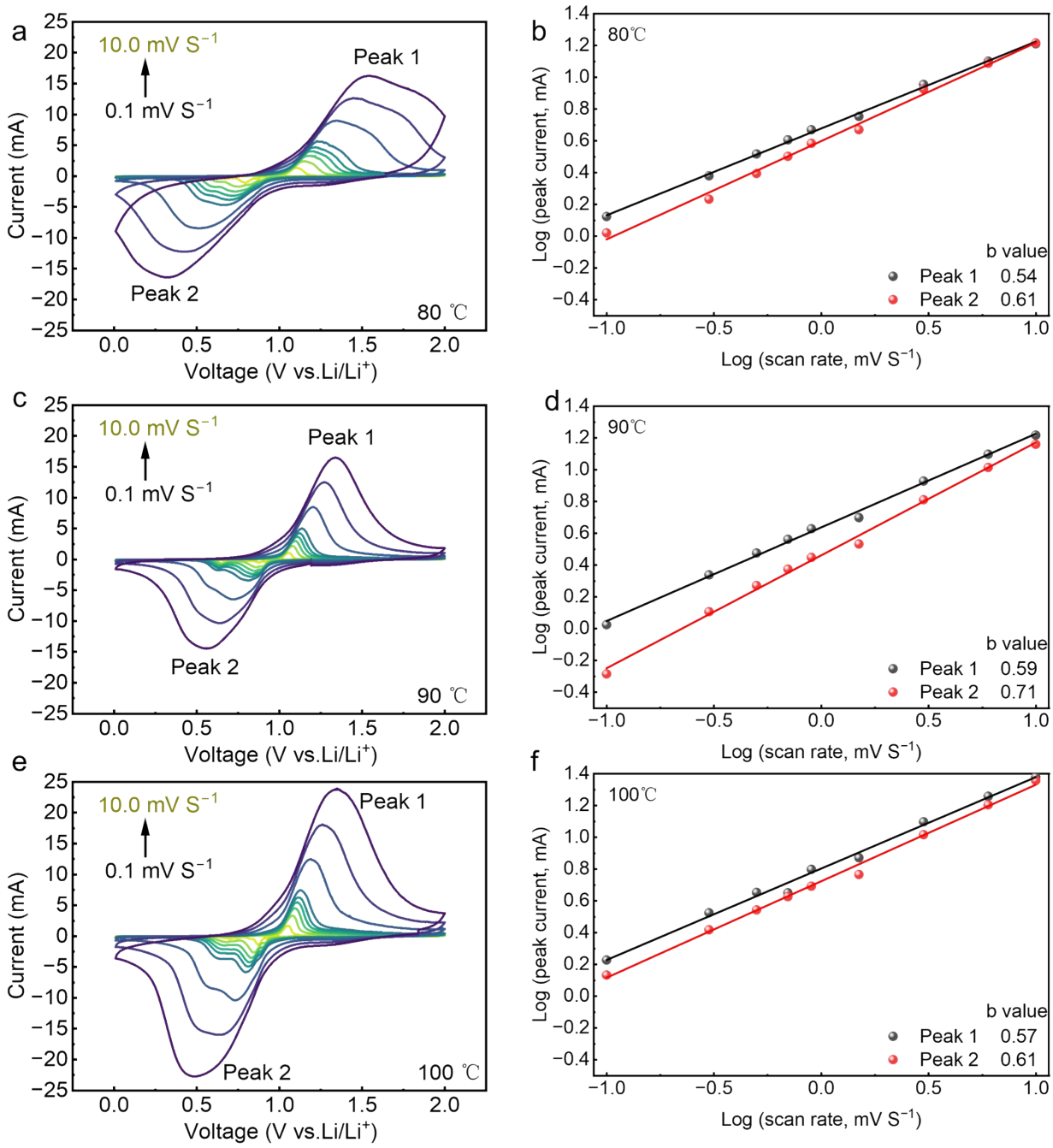

Figure S13. (a-c) kinetics of electrochemical reaction using CV at different scanning rates for 80, 90, and 100 °C.

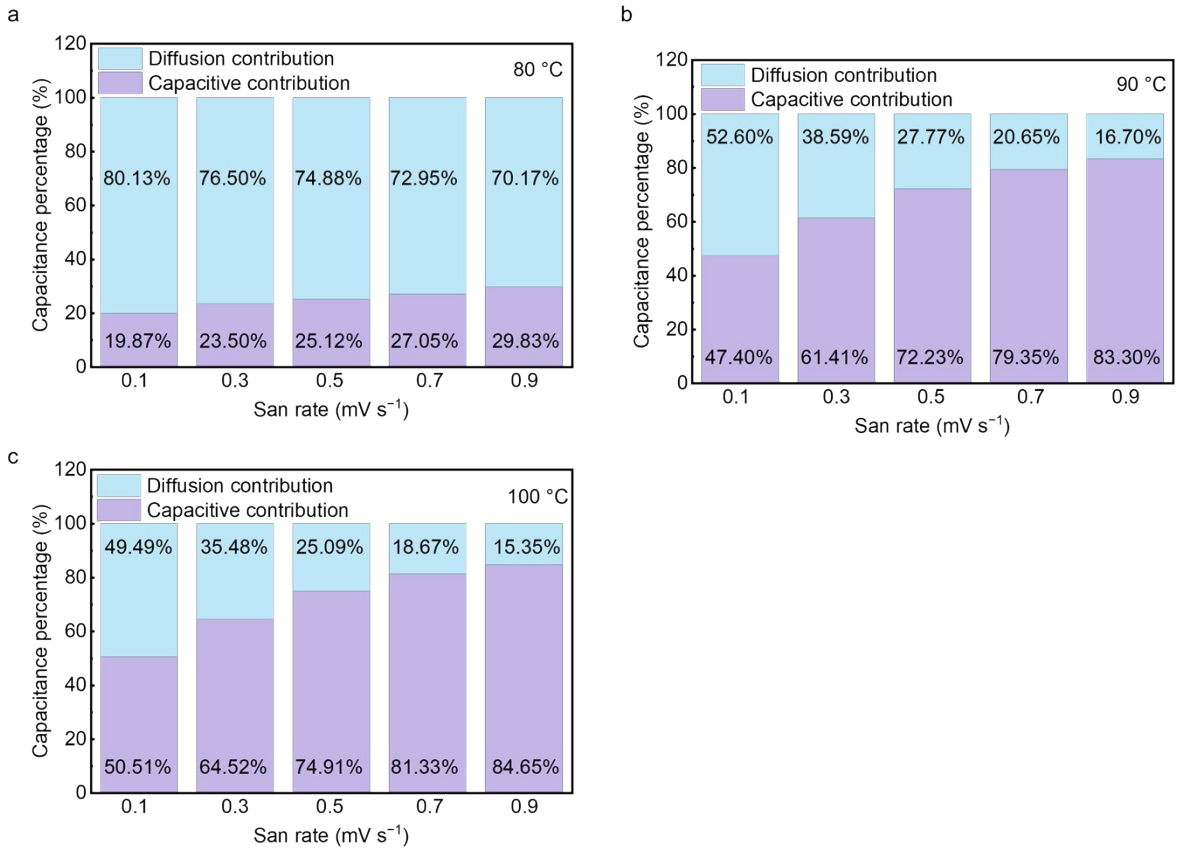

Figure S14. Contribution ratios of capacitive and diffusion currents at different scan rates (0.1, 0.3, 0.5, 0.7, and 0.9 mV s−1) for Li||Sb molten salt batteries at a) 80 °C, b) 90 °C, and c) 100 °C.

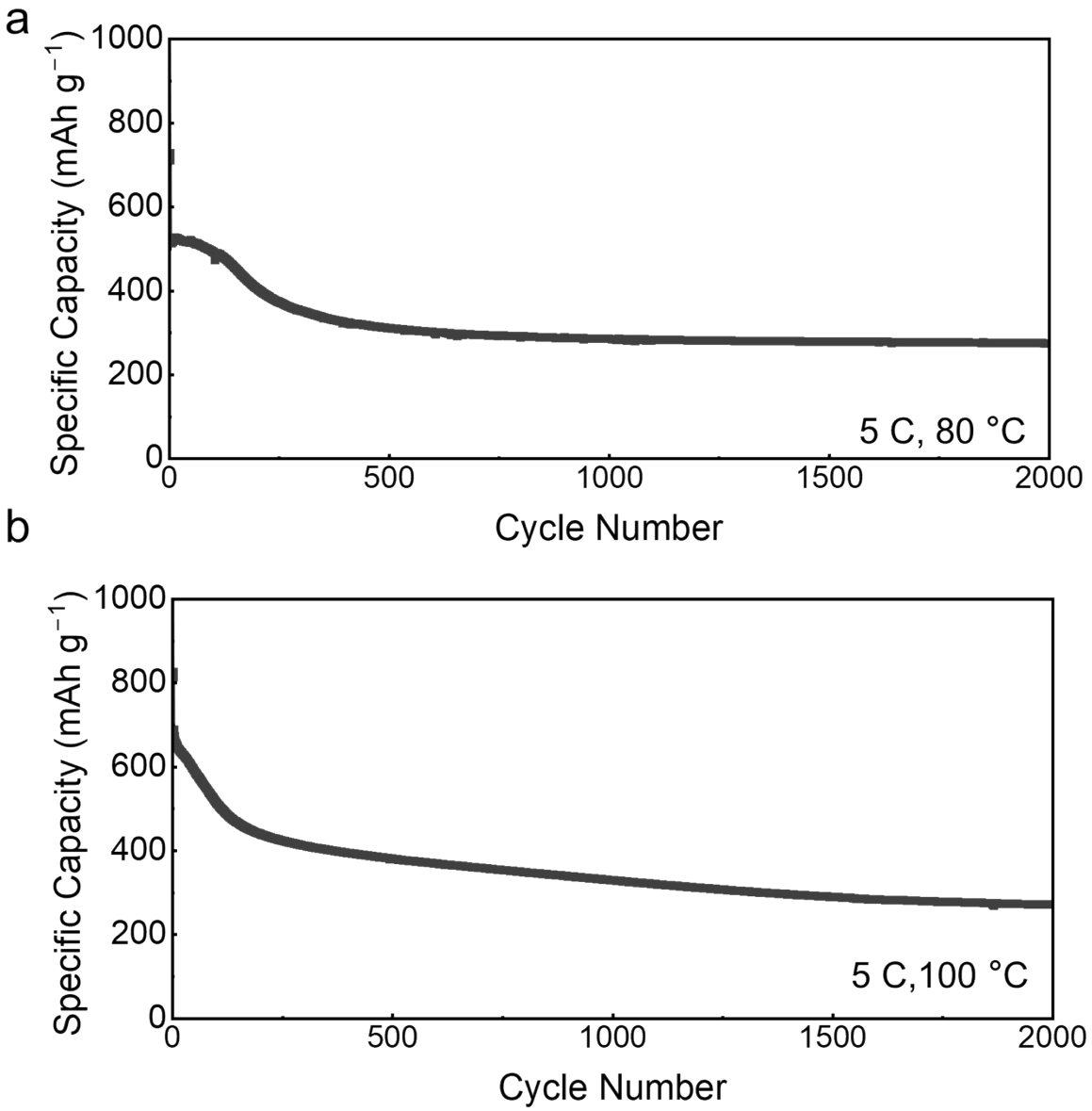

Figure S15. (a, b) Specific Capacity vs. Cycle Number at 5 C at 80 °C, and 100 °C of Li|||Sb molten salt batteries.

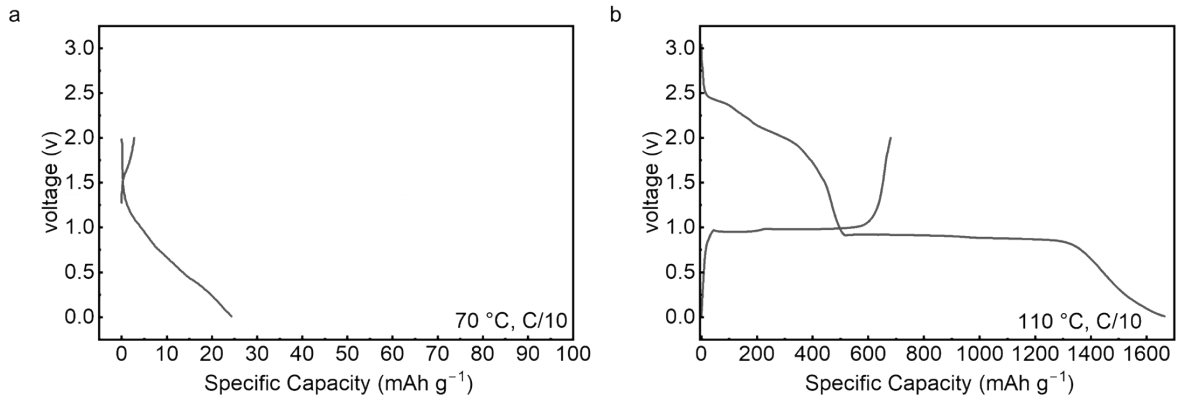

Figure S16. C/10 charge-discharge curves of Li||Sb molten-salt batteries at different temperatures. a) 70 °C; b) 110 °C.

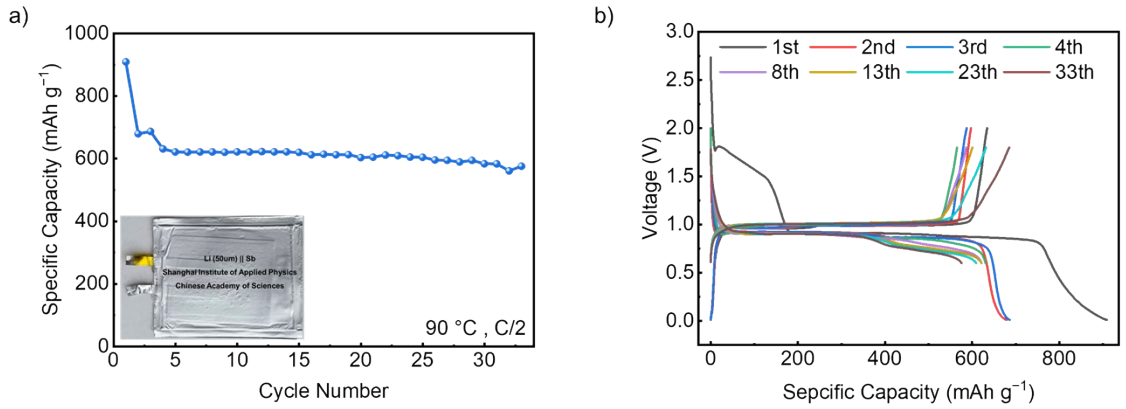

Figure S17. Performance of Li||Sb pouch cells at 90 °C. a) Plot of specific capacity versus cycle number; b) Charge-discharge curves. The pouch cell was initially activated for three formation cycles at C/10 between 0.01 and 2.0 V, followed by long-term cycling at 5 C within a voltage window of 0.6 to 1.8 V.

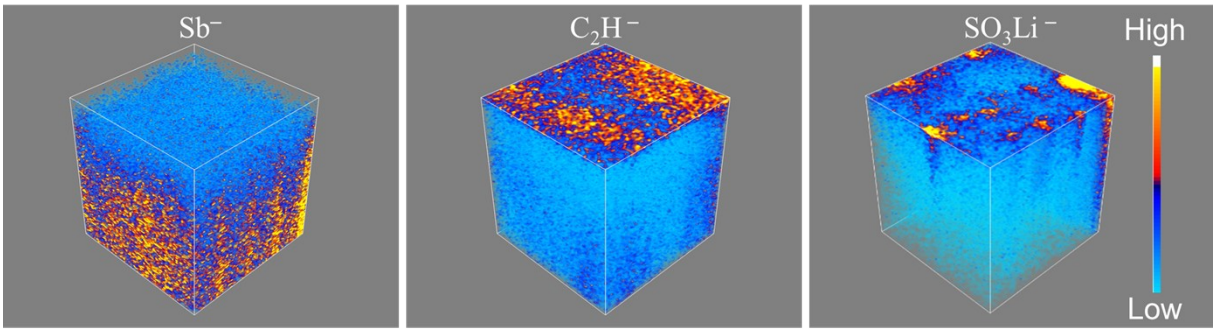

Figure S18. Time-of-flight secondary ion mass spectrometry (TOF-SIMS) elemental mapping of the Sb electrode after 100 cycles, showing the distribution of Sb^-, C_2H^-, and LiO_3S^- fragments.

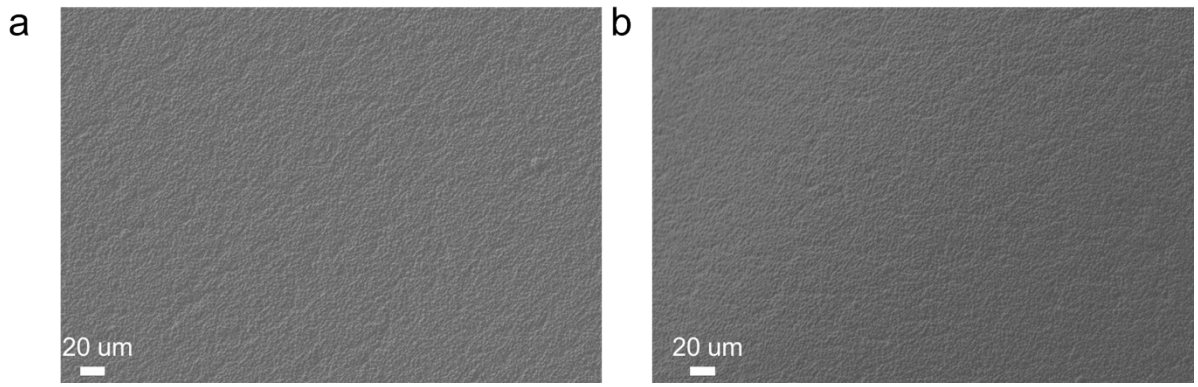

Figure S19. SEM images of (a) the pristine current collector and (b) the current collector after electrochemical cycling.

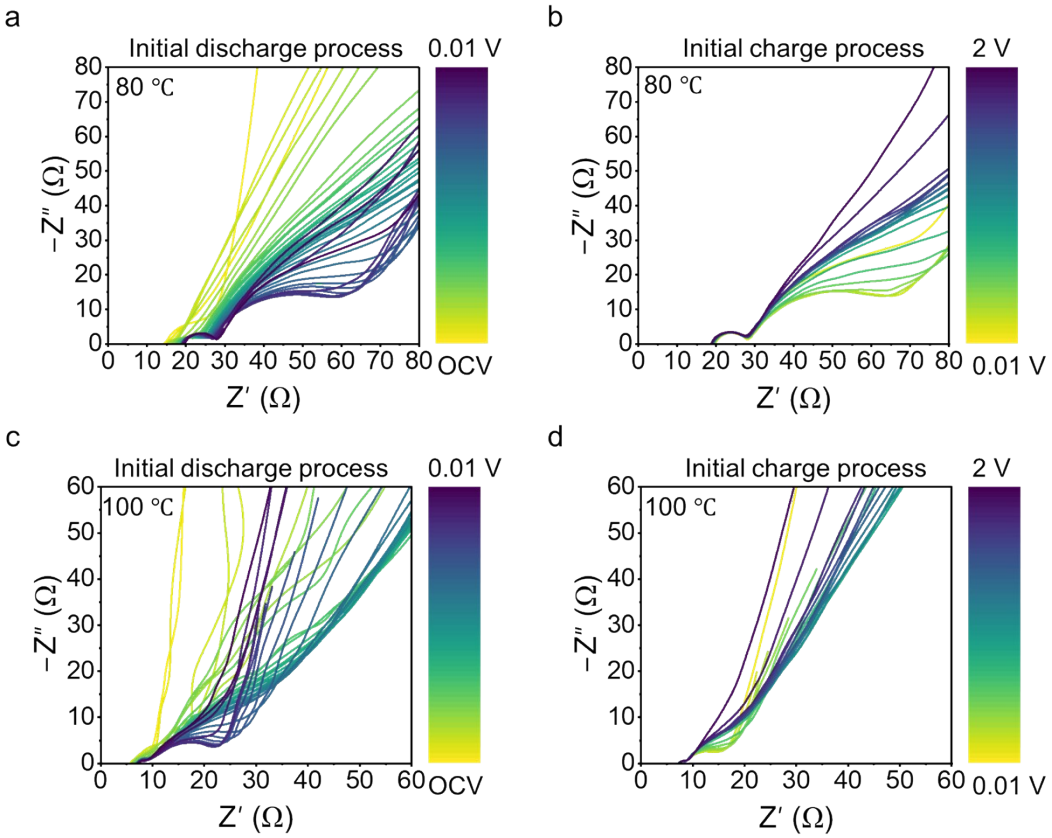

Figure S20. *In-situ* electrochemical impedance spectroscopy (EIS) of Li||Sb molten-salt batteries. Nyquist plots during the initial (a) discharge processes and (b) charge processes at 80 °C; and (c) discharge processes and (d) charge processes at 100 °C.